Chapter 2

Nanopyramid Structures with Light Harvesting and Self-Cleaning Properties for Solar Cells

Amalraj Peter Amalathas and Maan M. Alkaisi

Additional information is available at the end of the chapter

http://dx.doi.org/10.5772/intechopen.75314

Abstract

In this chapter, inverted and upright nanopyramid structures with light-harvesting properties and self-cleaning hydrophobic surfaces suitable for solar cells are presented. Periodic nanopyramid structures with 400–700 nm features were fabricated using interference lithography and combined dry and wet etching processes. The inverted nanopyramids (INP) were applied at the front side of the solar cells using UV nanoimprint lithography. These structures provided effective light-trapping properties and led to oblique angle light scattering and a significant reduction in reflectance resulting in higher power conversion efficiency. The second type, the periodic upright nanopyramid (UNP) structures were applied on a glass substrate by UV nanoimprint process. The glass cover is also utilized as a protective encapsulant front layer. The use of the upright nanopyramid structured cover glass in the encapsulated solar cell has also enhanced the power conversion efficiency due to the antireflection and strong light-scattering properties compared to the bare cover glass. In addition, the upright nanopyramid structured cover glass exhibited excellent self-cleaning of dust particles by rolling down water droplets. These results suggest that the nanopyramid structures with light-harvesting and self-cleaning properties can improve the performance of different types of solar cells, including thin films and glass-based PVs.

Keywords: solar cells, light-harvesting, self-cleaning, nanopyramids, laser interference lithography, nanoimprint lithography

1. Introduction

Reducing optical losses in the solar cells has always been a key factor in enhancing the conversion efficiency. In general, efficient light management has been achieved by textured

surfaces that enhance the light collection and increasing the effective optical path length of the light within the absorber layer of a solar cell [1]. Various texturing methods have been carried out such as texturing at the rear side [2] or the front side of a solar cell [3] or pre-texturing the thin film solar cell substrates [4, 5] in addition to the wide variety of light management schemes that are based on microscale structures that have been investigated to enhance the power conversion efficiency of solar cells. However, the use of nanostructures for improving the light absorption and trapping in solar cells is a more promising method compared to the traditional microsized surface texturing [6]. This is because of the lower level of induced damage and the ease of coating different surfaces and materials.

Nanostructures can be fabricated by various techniques, including electron beam lithography (EBL) [7], laser interference lithography (LIL) [8, 9], nanoimprint lithography (NIL) [10, 11], nanosphere lithography (NSL) [12] and block copolymer lithography (BCPL) [13]. Among them, the UV nanoimprint lithography (UV-NIL) is emerging as a powerful technique for fabricating nanoscale structures on large scale surfaces with simple, high-throughput, low-cost and high-resolution manufacturing capability [14]. Various nanostructures such as nanowires [15], nanorods [16], nanocones [17], nanopyramids [18], nanopillars [19] and metal nanostructures such as nanogrooves [20] and nanoparticle arrays [21] have been extensively studied. Despite their excellent light-trapping properties, texturing the active solar cell layer or introducing metal nanostructures within the cell results in poor charge carrier collection due to increased surface recombination. Fang Jiao et al. [22] demonstrated that the imprinting of moth-eye-like structures on the front side of monocrystalline Si solar cell surface enhanced the conversion efficiency by 19% compared to the planar solar cell through coupling the incident light into the absorber layer.

This chapter describes an approach of surface texturing which is different from other reported methods such as texturing the active material or using metal nanostructures. It is expected that nanopyramids coating approach might be enhanced solar cell performance without introducing additional surface recombination and excellent solar cell self-cleaning functionality.

Solar cell modules are installed in an outdoor environment for the vast majority of applications. Therefore, whatever the type of solar cell, glass is commonly incorporated as an encapsulation for preventing damage from dust, moisture and external shock [23, 24]. However, some of the incident light onto the solar cells will be lost through optical reflection due to the refractive index mismatch between the air and cover glass and through scattering or absorption by contaminants [25, 26]. In Section 2.3, it is shown that the amount of the incident light reaching the solar cell could be enhanced by incorporating antireflective and light-scattering nanostructures at the cover glass surface. Moreover, it is also demonstrated in Section 2.4 that the nanostructured cover glass has self-cleaning property and efficiently maintains the performance of solar cells in harsh environments.

The oblique light-scattering effect offered by the nanopyramids improves the light harvesting of the solar cells as a result of prolonged optical path length within the solar cells and thus, increasing the conversion efficiency [27, 28]. Several other research groups [29–31] have studied the use of cover glass that combines the antireflective and scattering effects with self-cleaning properties and examined their influence on the overall efficiency of the solar cells.

In this chapter, nanopyramid structures with light-harvesting properties and self-cleaning functionality are demonstrated on monocrystalline Si solar cells. Firstly, the fabrication process of coating monocrystalline solar cells with the periodic inverted or upright nanopyramid (UNP) structures using LIL and UV-NIL are presented. Secondly, the optical properties and surface wetting behavior of the upright nanopyramid (UNP) structured cover glass are presented. Also, the electrical performance of the solar cells with upright nanopyramid structured cover glass is examined in detail and compared to the performance of bare cover glass. Finally, the optical, electrical and wetting properties of the solar cells coated with the inverted nanopyramid (INP) structures are investigated.

2. Upright nanopyramid structured cover glass for solar cells

2.1. Fabrication of upright nanopyramid structures on a glass substrate

The UV nanoimprint lithography process is used for the replication of the upright nanopyramid (UNP) structures on glass substrates. The process flow diagram of the UV imprint is shown in **Figure 1**. First, the periodic inverted nanopyramid structures were formed on the Si master mold using laser interference lithography and subsequent pattern transfer process using reactive ion etching followed by KOH wet etching. Details of the fabrication process of the master mold are described in Ref. [9]. A UV curable resist (OrmoStamp) was spincoated onto a glass substrate and afterward the substrate was placed over the Si mold with the inverted nanopyramids inside the imprint tool. An imprint pressure of up to 4 mbar was applied to transfer the patterns with a

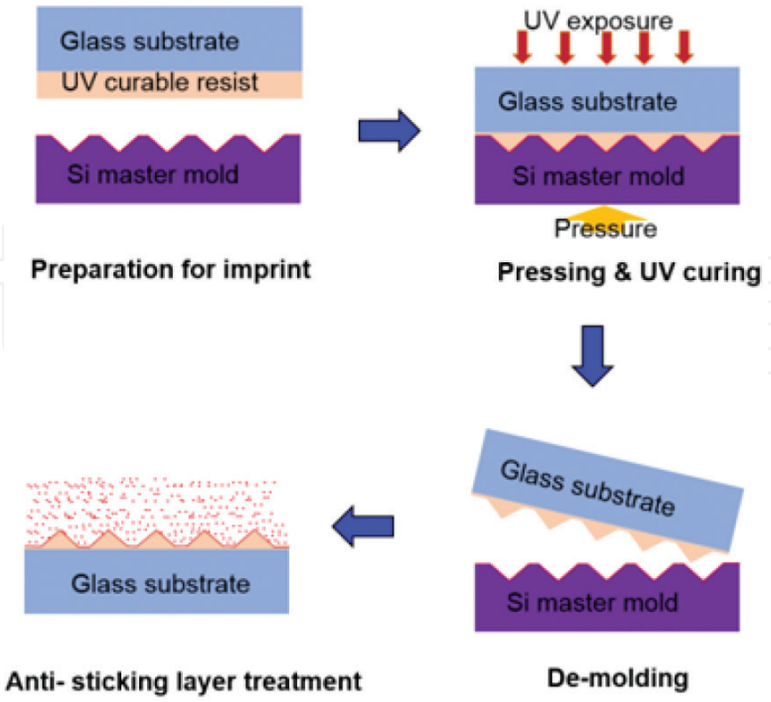

Figure 1. The schematic diagram of the overall fabrication process of upright nanopyramid structures on the glass.

UV light illumination of wavelength 365 nm. The upright nanopyramid pattern was successfully replicated from the Si mold onto the glass substrate with high fidelity. After the UV nanoimprint process, F_{13}-TCS-based SAM was coated onto the upright nanopyramid patterned glass substrate in order to increase the hydrophobicity of the surface. More details of the UV nanoimprint process parameters and the tools which were employed can be found in Ref. [32].

The surface morphologies of the inverted and upright nanopyramid structures were examined by using scanning electron microscope (SEM) (JEOL 7000F FE-SEM) and atomic force microscope (AFM, DI3000). **Figure 2(a)** and **(c)** presents the SEM images and AFM image of the Si master mold with inverted nanopyramid structures, respectively. **Figure 2(b)** and **(d)** shows the SEM images and AFM images of the upright nanopyramid structured glass replicated from the master mold, respectively. As illustrated in **Figure 2(b)**, the inverted nanopyramid patterns on the Si master mold were transferred onto the UV curable resist coated glass substrate without any distortion and deformation using UV nanoimprint lithography. This is also confirmed in the AFM image in **Figure 2(d)**. As shown in **Figure 2**, the 450 nm wide and 310 nm high UNP structures with 125 nm separation were replicated uniformly over an area of 10x10 mm after the imprint process.

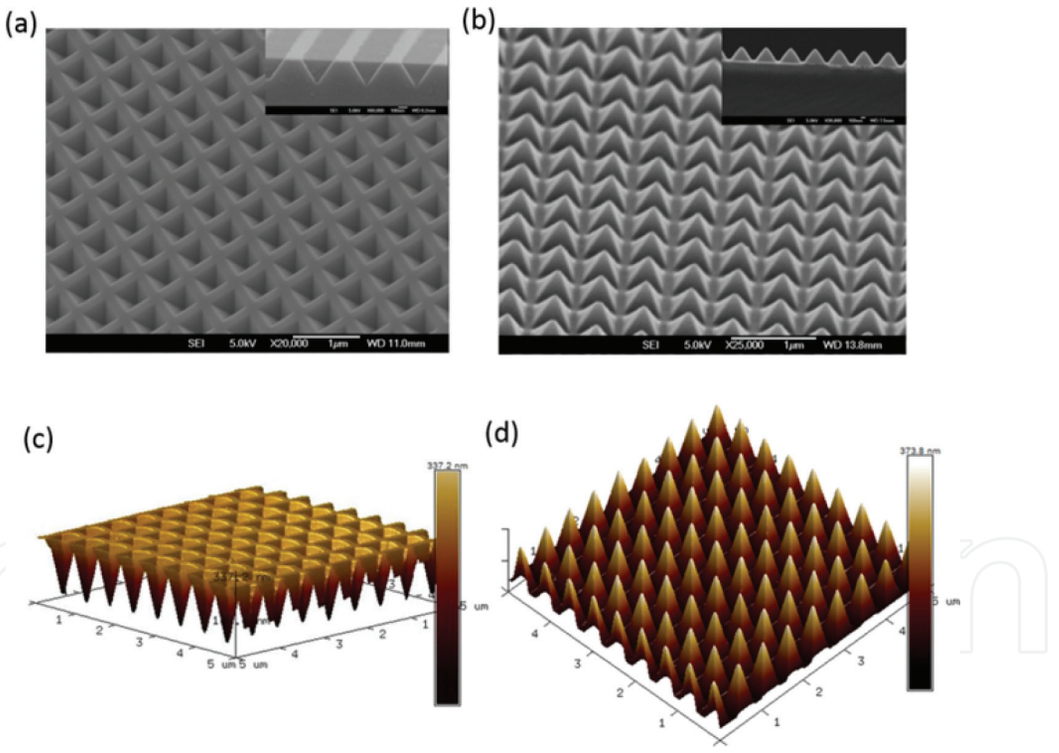

Figure 2. 30°-tilted view SEM images of (a) inverted nanopyramid Si master mold and (b) upright nanopyramid structured on the glass, and the inset images are the cross-sectional views of SEM images. Three-dimensional AFM images (c) inverted nanopyramid Si master mold and (d) upright nanopyramid structured glass.

2.2. Solar cell fabrication

Monocrystalline Si solar cells were fabricated by the process shown in **Figure 3**. A single-side-polished, Czochralski (CZ) grown, 350 μm thick, boron doped p-type silicon wafer with <100>

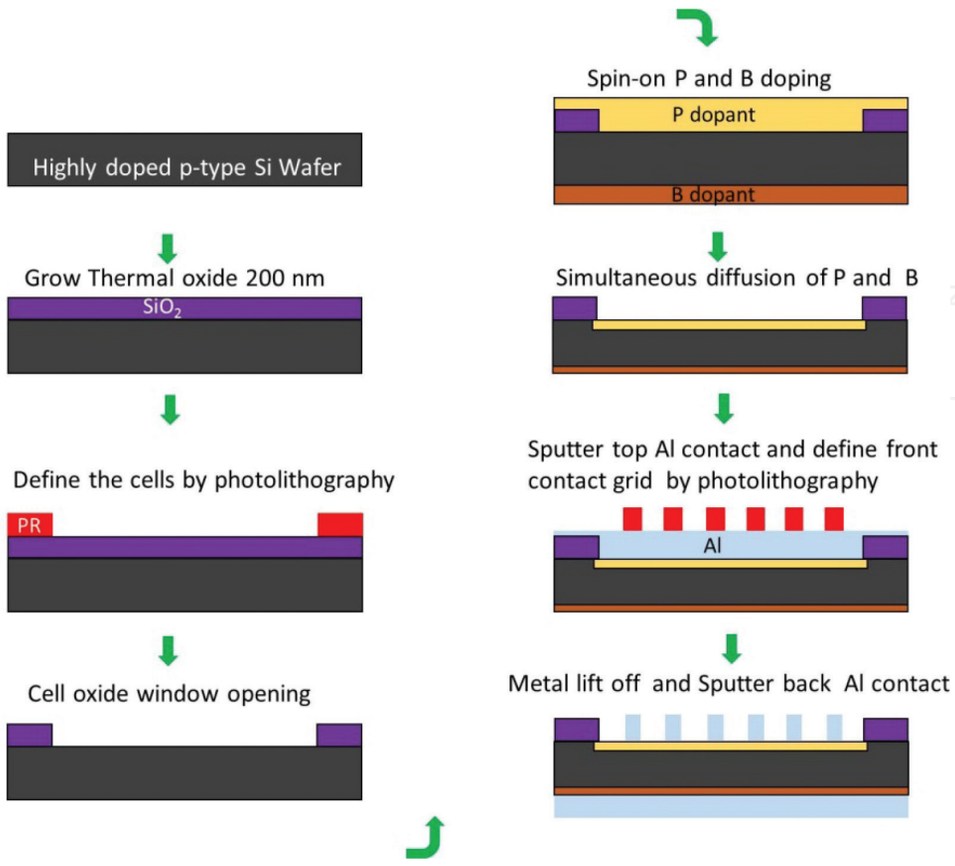

Figure 3. The schematic representation of monocrystalline Si solar cell fabrication process.

crystal orientation and resistivity of 0.5–1.0 Ωcm was used as the substrate. After piranha cleaning and 1:10 dilute HF dipping, a 200 nm thermal oxide was grown on the wafer using quartz tube furnace and dry/wet oxidation was done at 1000°C. The 10 mm × 10 mm individual cells were defined by photolithography, and buffered HF etching was performed to isolate the individual cells by opening windows in the oxide. The wafer backside was doped with boron dopant (B202 form Filmtronics) to create the back surface field effect. The emitter junction was formed by spin-on phosphorus doping processes using P509 dopant from Filmtronics. The diffusion was performed in a quartz tube furnace at 950°C for 30 min in a 20% O_2 and 80% N_2 environment. The phosphosilicate glass (PSG) on the wafer surface was removed using the diluted 10% HF solution. The 300-nm thick aluminum front and back contact were deposited by DC sputtering. In creating the top contact, top contact patterns were defined by photolithography before the metal deposition.

2.3. Optical properties and device performance

The total and diffuse transmittance of UNP patterned glass or unpatterned bare glass were measured using a UV–visible spectrophotometer at room temperature with an integrating sphere over the wavelength range of 300–1200 nm. **Figure 4(a)** illustrates the comparison between the total and diffuse transmittance of the glass substrates with and without UNP patterns, which were measured using an integrating sphere with the incoming light entered from the patterned glass substrate side. As shown in **Figure 4(a)**, the total transmittance of the

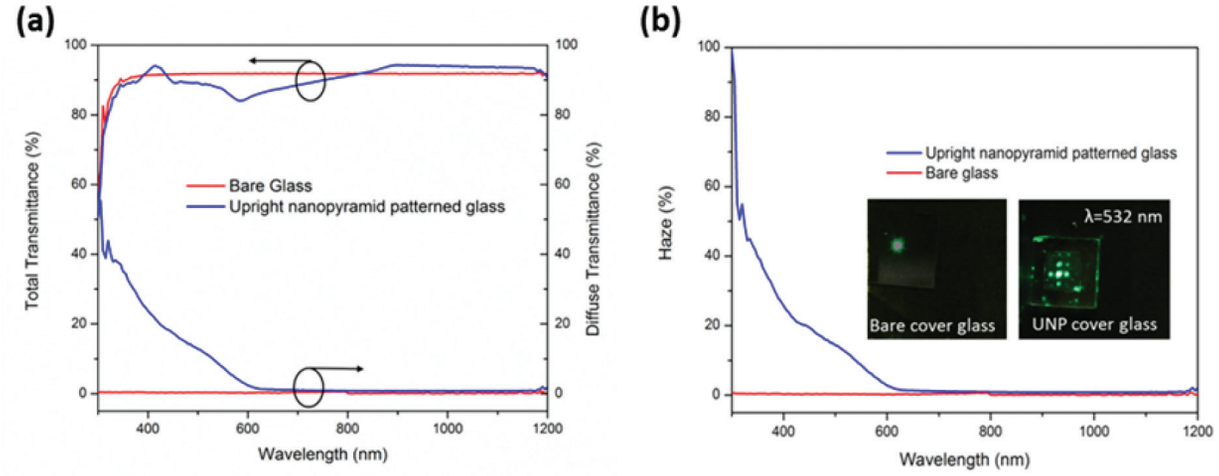

Figure 4. (a) Measured total and diffuse transmittance spectra of the bare glass and the UNP patterned glass as a function of wavelength and (b) the optical haze spectra of the bare glass and the UNP patterned glass as a function of wavelength. Photographs of diffracted light patterns of the corresponding samples obtained from the green diode laser with a wavelength of 532 nm are also displayed in the inset.

UNP patterned glass was slightly lower than that of the bare glass in the wavelength range of 450–800 nm which may be caused by the diffraction losses due to the higher order diffracted waves [33, 34]. However, the diffuse transmittance of the UNP patterned glass was increased up to 24% in the visible wavelength region due to higher orders of diffracted waves in the transmission, whereas the bare glass substrate shows almost no diffuse transmittance over a wide wavelength range as illustrated in **Figure 4(a)**.

The haze value (H), which is determined by the ratio of the diffuse transmittance (T_d) to the total transmittance (T_t), that is, $H = T_d/T_t$, indicates the light-scattering properties of the samples. When the incident light passed through the bare cover glass, the H value is close to zero as shown in **Figure 4(b)**. In contrast, the H value is significantly increased for patterned glass, especially, in the wavelength range 300–600 nm, which signifies that strong light scattering is achieved by UNP structured glass. This light-scattering behavior can also be confirmed in the insets of **Figure 4(b)**. For the bare cover glass, there is almost no light diffraction, whereas the UNP patterned glass shows high order diffraction patterns using a green diode laser at a wavelength of 532 nm. This scattering effect will result in changes in the propagation direction of light from normal to the oblique incidence in the solar cell. As a result, the optical path length of the incident light is elongated, and hence the light absorption in the active layer of the solar cell is also improved by the patterned glass. Indeed, the high haze optical property due to the light scattering effect would positively enhance the power conversion efficiency of the solar cells with the UNP patterned glass compared to the bare cover glass [35–37]. This is especially important for thin film devices.

Numerical simulations were performed using the finite-difference time-domain (FDTD) method by Lumerical solutions Inc. to illustrate how the incoming light couples with and without upright nanopyramid structure. **Figure 5** shows the FDTD simulation model layout of the UNP structured glass substrate in perspective view and XZ view. Perfectly matched layers (PML) and periodic boundary conditions were used in the perpendicular and horizontal directions.

http://dx.doi.org/10.5772/intechopen.75314

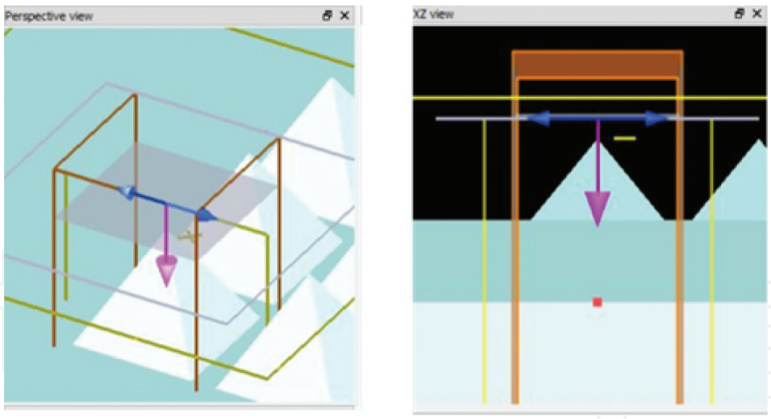

Figure 5. FDTD simulation model layout of the UNP structured glass substrate: (a) perspective view and (b) XZ view.

The cross-sectional electric field distributions at different wavelength obtained for the incident light propagating from air to the glass substrate with and without upright nanopyramid structure are depicted in **Figure 6**. As shown in **Figure 6**, upright nanopyramid structures show wide angular range light-scattering patterns, especially in the wavelength range below 600 nm and provide oblique light transmission from air and the glass while there is no scattering of light for bare cover glass. These results demonstrate that the upright nanopyramid structured

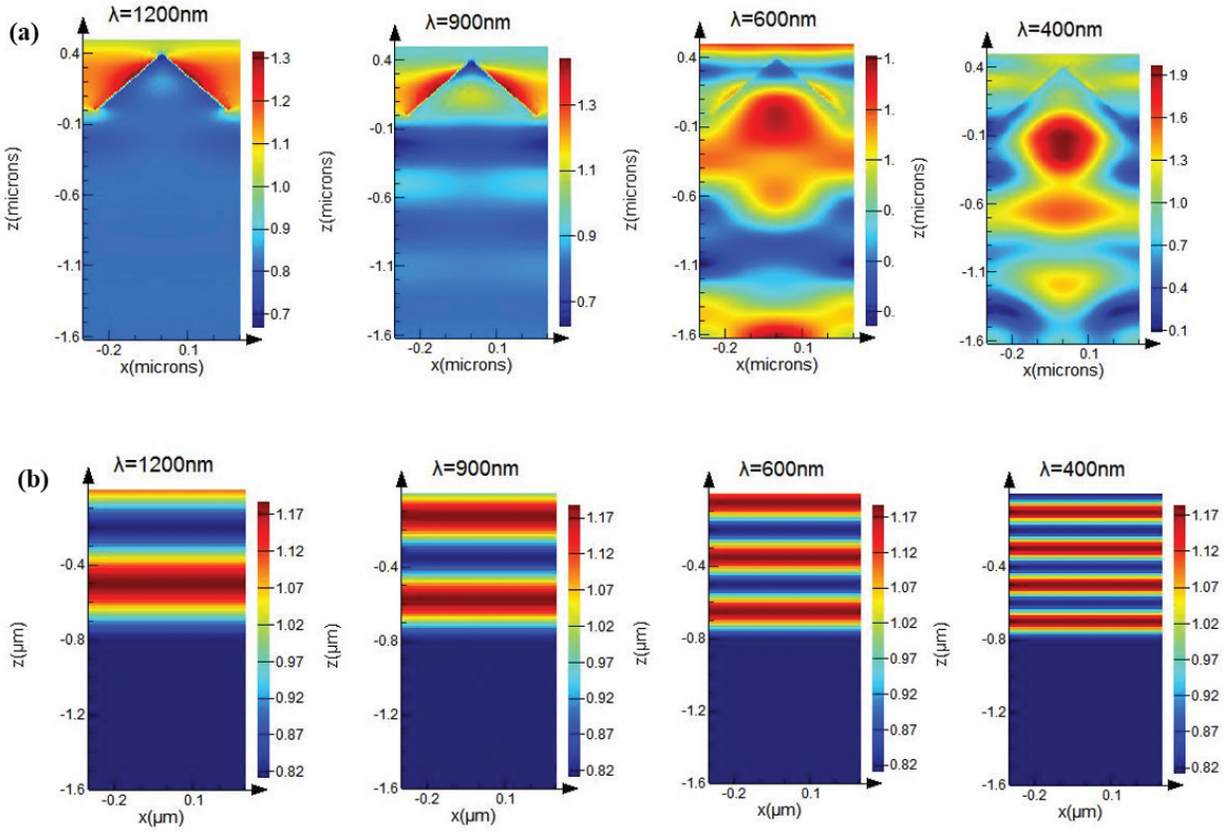

Figure 6. The cross-sectional electric field distribution profiles at different wavelength by FDTD analysis: (a) upright nanopyramid structured glass with a period of 600 nm, base of 500 nm and height of 400 nm and (b) bare flat glass.

glass enhances the diffuse transmittance of the cover glass or any substrate used for solar cells applications. Thus, these structures can lead to the power conversion efficiency enhancement of encapsulated solar cells due to the improved light harvesting in the absorption layer of the solar cells caused by the combined effects of strong light scattering and antireflection coating [37, 38].

In order to verify the effect of the periodic upright nanopyramid patterns, the patterned glass and the bare glass substrate were employed as a cover encapsulation glass on the monocrystalline Si solar cell. **Figure 7(a)** shows the current density-voltage characteristics of the encapsulated monocrystalline Si solar cell with and without UNP patterned cover glass. The monocrystalline Si solar cell performances are summarized in **Table 1**.

There was no significant change in the open circuit voltage (V_{OC}), but a significant enhancement in the short-circuit current density (J_{SC}) was observed as expected. The fill factor (FF) of monocrystalline Si solar cell was slightly enhanced from 55.23 to 59.76% with UNP patterned cover glass. Such improvement in FF could be attributed to the enhanced density of free carriers [39] induced by the increased number of photons entering the active layer of the solar cell and reducing the effective series resistance. The value of J_{SC} for the monocrystalline Si solar cell without cover glass was 34.38 $mAcm^{-2}$. This value was decreased to 31.60 $mAcm^{-2}$ with a bare cover glass. This reduction in J_{SC} indicates that the cover glass reduces the number of photons entering the active layer of the solar cell through reflection and absorption processes. However, by replacing the bare glass with UNP patterned cover glass, J_{SC} value was increased to 32.39 $mAcm^{-2}$ for encapsulated monocrystalline Si solar cell. Hence, the use of the upright nanopyramid patterned glass as a cover glass is an effective way to improve the power conversion efficiency (PCE). The encapsulated monocrystalline Si solar cell with patterned glass efficiency has increased by 10.97% compared to the encapsulated monocrystalline Si solar cell with bare cover glass. The experiment was repeated with commercially manufactured polycrystalline solar cell and similar trend was observed. This enhancement is mainly due to the strong light scattering effect via the upright nanopyramid structures.

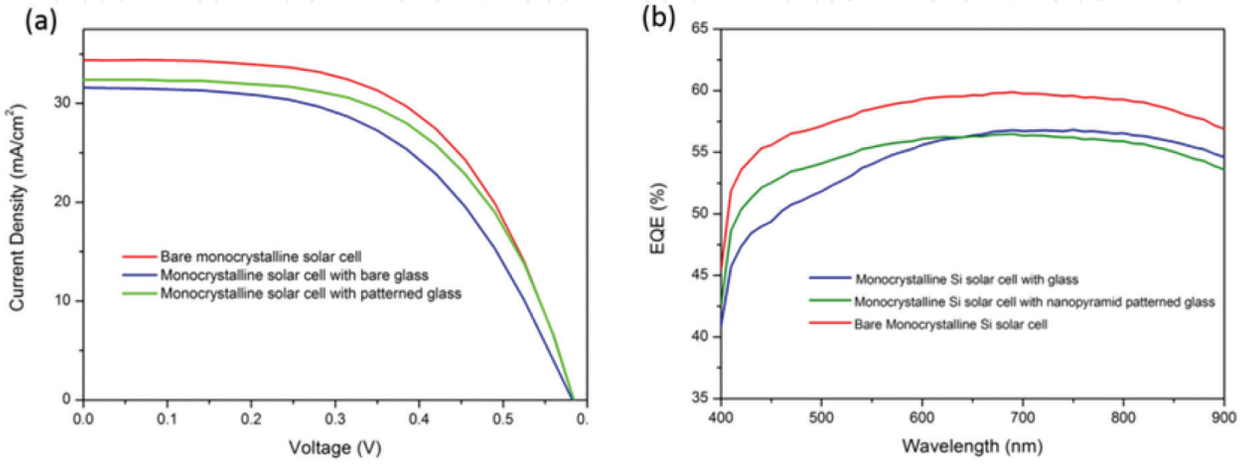

Figure 7. (a) Current density-voltage characteristics and (b) external quantum efficiency (EQE) spectra of encapsulated monocrystalline Si solar cell with and without the upright nanopyramid patterned cover glass and bare cover glass.

Monocrystalline Si solar cells	V_{OC} (V)	J_{SC} (mAcm^{-2})	FF (%)	PCE (%)
Without cover glass	0.58	34.38	59.82	11.93
Bare cover glass	0.58	31.60	55.23	10.12
UNP patterned cover glass	0.58	32.39	59.76	11.23

Table 1. Device characteristics of encapsulated monocrystalline Si solar cells with and without the UNP patterned cover glass and the bare cover glass.

As shown in **Figure 7(b)**, the solar cells with upright nanopyramid patterned cover glass exhibited improved EQE values in comparison with the bare cover glass, particularly in the wavelength region of 400–600 nm. This is due to the increased photogenerated carriers generated by its higher haze properties. This result was precisely matched with the optical haze value result shown in **Figure 4**. From these results, the periodic upright nanopyramid patterned glass offers a better-graded index medium to the incident light compared to the bare glass [25]. Therefore, the patterned cover glass can reduce the Fresnel reflectance and scatter more incident light into the solar cells' emitter area and prolong the optical path length, therefore, improving the light trapping and increasing the overall conversion efficiency.

2.4. Surface wettability and self-cleaning behaviors

In real outdoor environments, the cover glass layer of the solar cell can easily be contaminated by dust particles which interfere with the incident light directed into the solar cell active layer and thus reducing the solar cells' performance. Therefore, the nanopyramids covered glass encapsulation has the advantages of acting as an antireflection layer and as self-cleaning surface and will maintain the solar cell performance under real outdoor environment condition [40, 41]. The water wetting behaviors of the samples with different morphologies were investigated. **Figure 8** shows (a) the photographs of a water droplet on (I) the bare glass, (II) UNP structured glass and (III) SAM-coated UNP structured glass and (b) sequential photographs of water droplet self-cleaning process for (I) the bare cover glass and (II) UNP structured glass.

As shown in **Figure 8(a)**, the bare glass exhibited a hydrophilic surface with a water contact angle (θ_{CA}) of ~36° while UNP patterned glass showed a hydrophobic behavior with a θ_{CA} value of ~112°. This hydrophobic behavior is associated to the enhanced surface roughness of the UNP patterned glass, which can be demonstrated by the Cassie-Baxter Equation [42]. Moreover, F_{13}-TCS-based SAM was coated onto the UNP patterned glass in order to enhance its hydrophobic surfaces. In this case, the contact angle of the SAM-coated UNP glass was increased to 132° as shown in **Figure 8(a)**. These contact angle ($\theta_{CA)}$ values are comparatively lower than those reported with superhydrophobicity (i.e., $\theta_{CA} > 150°$) in previous studies [43, 44]. However, it can be observed that the black dust particles on the surface of UNP patterned glass were cleared away by the rolling down water droplets without any remaining dust particles or water droplets at the surface, as shown in **Figure 8(b)**. In contrast, the dust particles remained on the bare glass even with rolling down water droplets. Thus, the dust particles partially remained especially at the edge of the bare glass. The conclusion is that the UNP patterned cover glass has dual functionality of light-harvesting and self-cleaning properties and would enhance the practicability of solar cells in real outdoor environments.

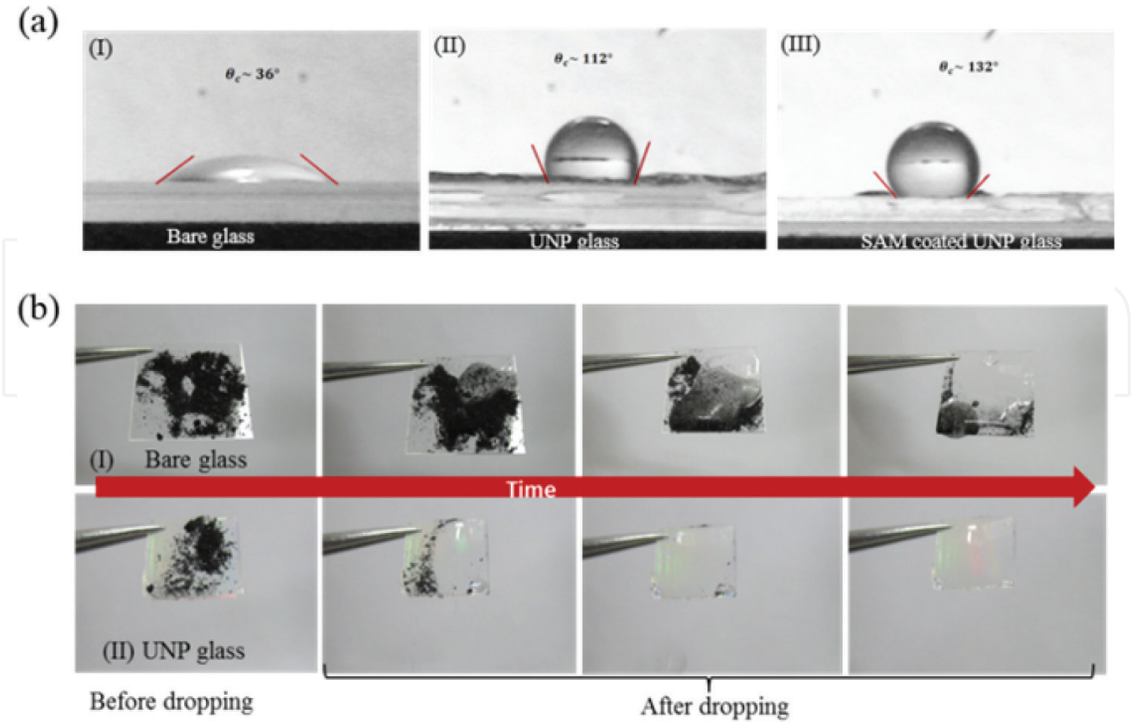

Figure 8. Photographs of (a) a water droplet on (I) bare glass, (II) UNP glass and (II) SAM-coated UNP glass and (b) sequential photographs of a self-cleaning process for (I) the bare glass and (II) UNP glass. θ_{CA} is the water contact angle.

3. Inverted nanopyramid structures

3.1. Fabrication of inverted nanopyramid structures by UV-NIL

Figure 9 illustrates the schematic diagram of overall imprint process steps for the coating of inverted nanopyramid structures on a solar cell front surface. The periodic inverted nanopyramid structures were fabricated on Si master mold by LIL and subsequent pattern transfer process using reactive ion etching followed by KOH wet etching. Details on the fabrication process of the master mold are described in Ref. [9]. The upright nanopyramid patterns were successfully replicated from the Si mold onto the glass substrate using UV nanoimprint process resulting in high fidelity as described in Section 2.1. The upright nanopyramid structured glass was used as a stamp in the second imprint process to produce the inverted nanopyramid patterns. After the UV nanoimprint process, F_{13}-TCS-based SAM was coated onto the upright nanopyramid patterned glass substrate to act as an anti-sticking layer. More details of the UV nanoimprint process parameters and the tools which were used are described in Ref. [11].

In order to determine and measure the influence of the inverted nanopyramid structure on improving the solar cell conversion efficiency, the inverted nanopyramid structures were printed onto monocrystalline Si solar cells. The monocrystalline Si solar cells were fabricated as described in Section 2.2. **Figure 10(a)** shows the top view SEM images of the periodic inverted nanopyramid Si master stamp. The upright nanopyramid replica stamp (**Figure 10(b)**)

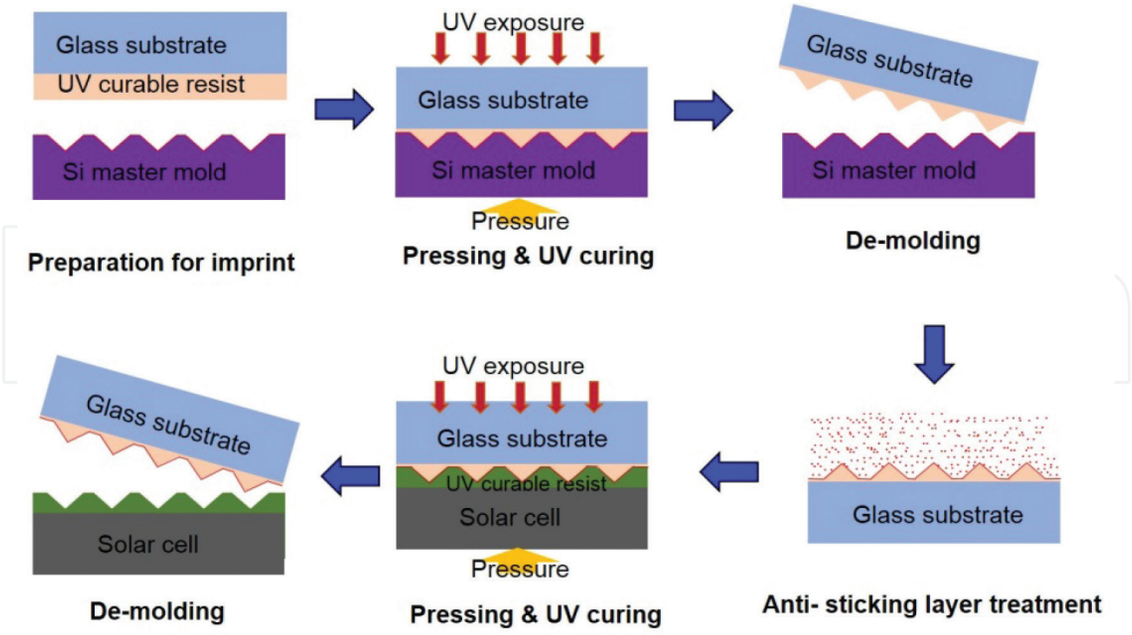

Figure 9. The schematic diagram of the overall fabrication process of inverted nanopyramid structures on the front surface of the solar cells.

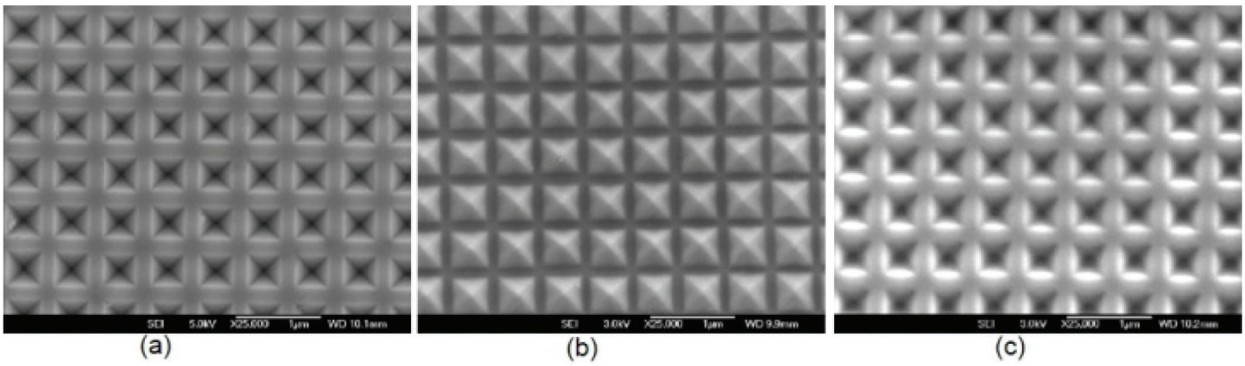

Figure 10. Top view of SEM image of: (a) the inverted nanopyramid Si master mold, (b) the upright nanopyramid replica stamp and (c) the periodic inverted nanopyramid imprinted from the upright pyramids mold on the front surface of the solar cells.

was imprinted from the master Si stamp (**Figure 10(a)**). The periodic inverted nanopyramid imprinted onto the surface of the solar cells (**Figure 10(c)**) was obtained from the upright nanopyramid replica stamp. It can be seen that the inverted nanopyramid structures were transferred to the surface of the solar cell with high fidelity.

3.2. Optical properties and device performance

Figure 11 shows the reflectance of the monocrystalline Si surface with and without the coating of inverted nanopyramid structures measured as a function of wavelength. It can be observed that the surface reflectance of the monocrystalline Si with the inverted nanopyramid layer was significantly decreased over the broad wavelength ranging from 300 nm to

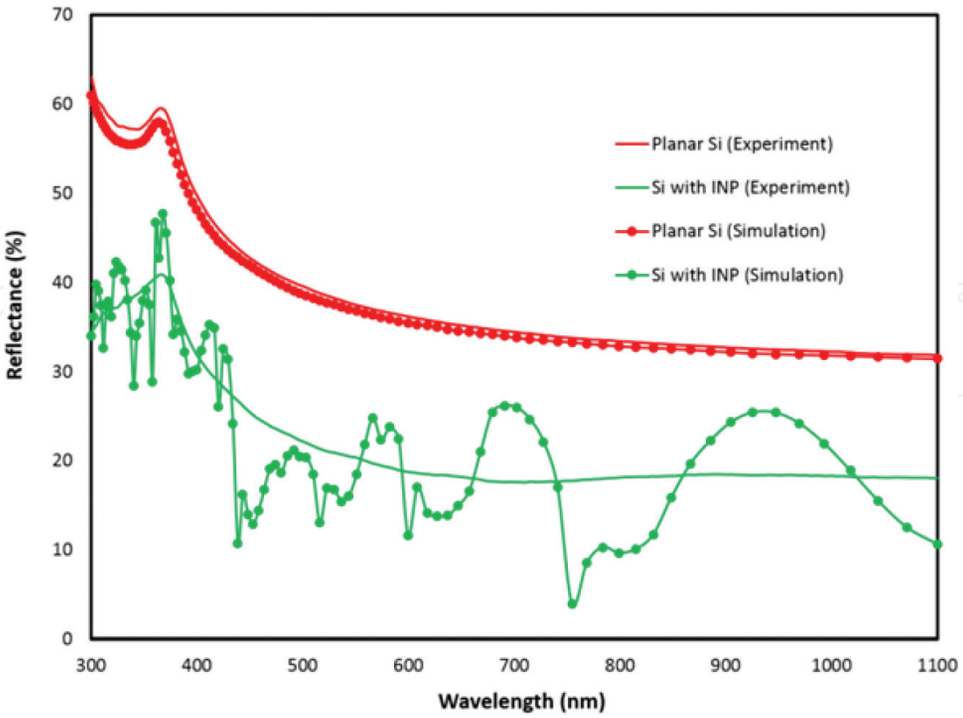

Figure 11. Experimental and FDTD-simulated optical reflectance spectra of Si surface with and without INP structure as a function of wavelength.

1200 nm due to the gradual change in the refractive index between the air and Si surfaces. This is compared with the planar solar cells with no nanopyramid pattern (red curve in **Figure 11**), which resulted in 40% reflections over the visible range.

FDTD simulations were performed with and without inverted nanopyramid structure to verify the reflection attained from the experiments, resulting in simulated reflectance spectra, as also illustrated in **Figure 11**. It is apparent that the theoretical reflection measurement for planar Si substrate is close to the experimental results. The overall trend of simulated reflectance spectra is quite consistent with that of the experiment data, with noticeable decrease of reflectance for inverted nanopyramid structures. Concurrently, the fluctuations of the reflectance can be associated with the limitation of the modeling where the OrmoStamp layer is assumed to have a uniform refractive index over the broad wavelength range under study. Moreover, the cross-sectional electric field intensity distributions at different wavelengths were simulated for incident light propagating from air to the Si substrate with and without inverted nanopyramid structure as shown in **Figure 12**.

As shown in **Figure 12**, the existence of inverted nanopyramid structure results in less intensity and weaker interference of the reflected waves. Hence, these structures are suitable antireflection coatings. In addition, it can be observed from the strong electric field distribution inside the inverted nanopyramid structure that the EM wave energy can be effectively coupled to the inverted nanopyramid structures. This is because more incident photons are coupled to the device due to the formation of a gradual refractive index gradient profile provided by the inverted nanopyramid structure.

http://dx.doi.org/10.5772/intechopen.75314

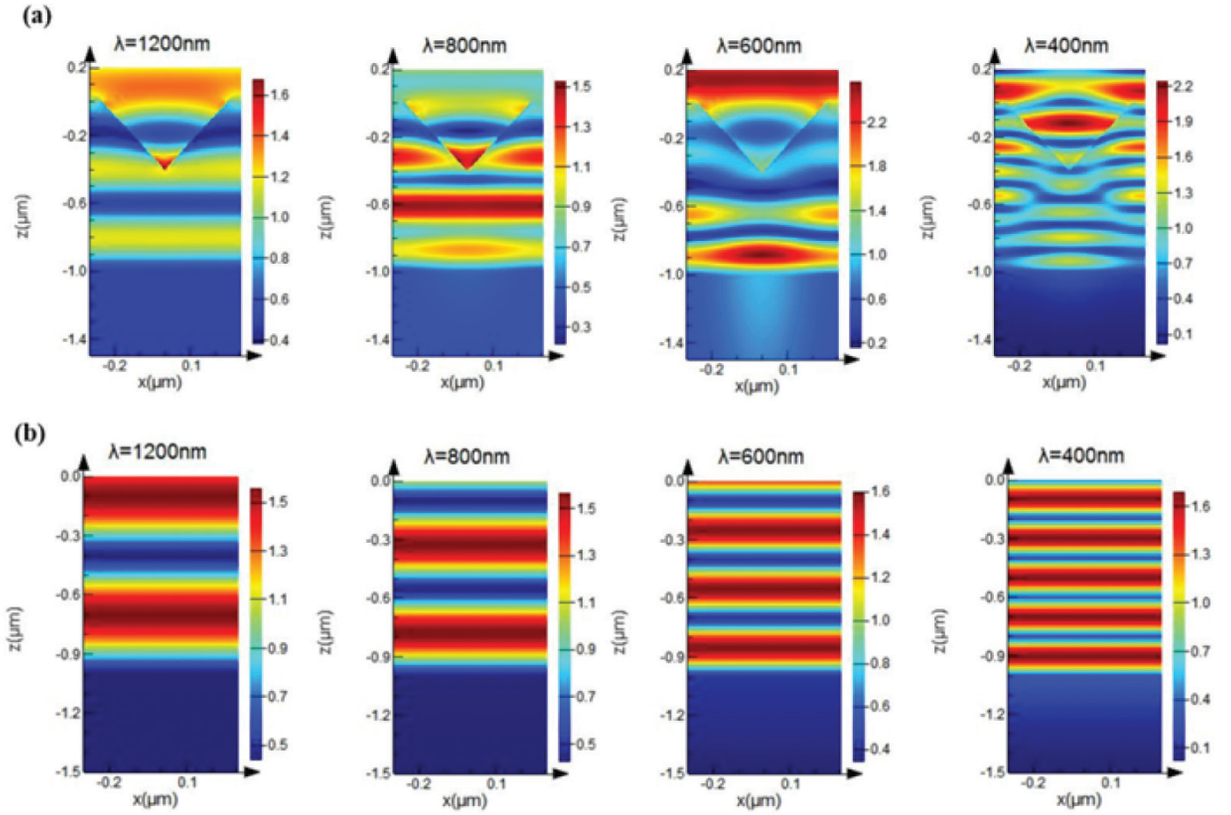

Figure 12. The cross-sectional electric field distribution profiles at different wavelengths employing FDTD analysis (a) INP coated Si with a period of 600 nm, the base size of 500 nm and depth of 400 nm and (b) planar Si subjected to same light conditions.

Figure 13(a) and **(b)** shows the J-V characteristics and EQE spectra of the monocrystalline Si solar cell with and without the inverted nanopyramid structures. The photovoltaic parameters of the monocrystalline Si solar cells with and without nanopyramid structures extracted from these J-V curves are summarized in **Table 2**.

With the use of inverted nanopyramid structures, the J-V characteristics show that there was no significant change in the open circuit voltage (V_{OC}). However, the short-circuit current density (J_{SC}) of planar monocrystalline Si solar cell increased from 29.422 to 32.793 $mAcm^{-2}$. This J_{SC} increment was mainly due to the reduced reflectance resulting from the inverted nanopyramid structure over a broad wavelength range as shown in **Figure 11**. As a result, the conversion efficiency of the monocrystalline Si solar cell with inverted nanopyramid was increased significantly from 8.122 to 9.075%. This efficiency is 11.73% higher than the one obtained for the planar, not patterned, monocrystalline Si solar cell. The EQE measurement is carried out under a monochromatic illumination with a tungsten-halogen lamp coupled to a monochromator. The EQE values of the tested monocrystalline Si solar cell with inverted nanopyramid layer were significantly higher over the entire wavelength range compared to the non-patterned solar cells. For instance, the EQE value increased by about 8% at wavelength of 450 nm. This higher EQE values for the solar cells with inverted nanopyramid indicate enhanced light trapping and reduced reflections due to the imprinted nanostructures on top of the solar cell surface. This result is precisely matched with the reflectance values obtained in **Figure 11**.

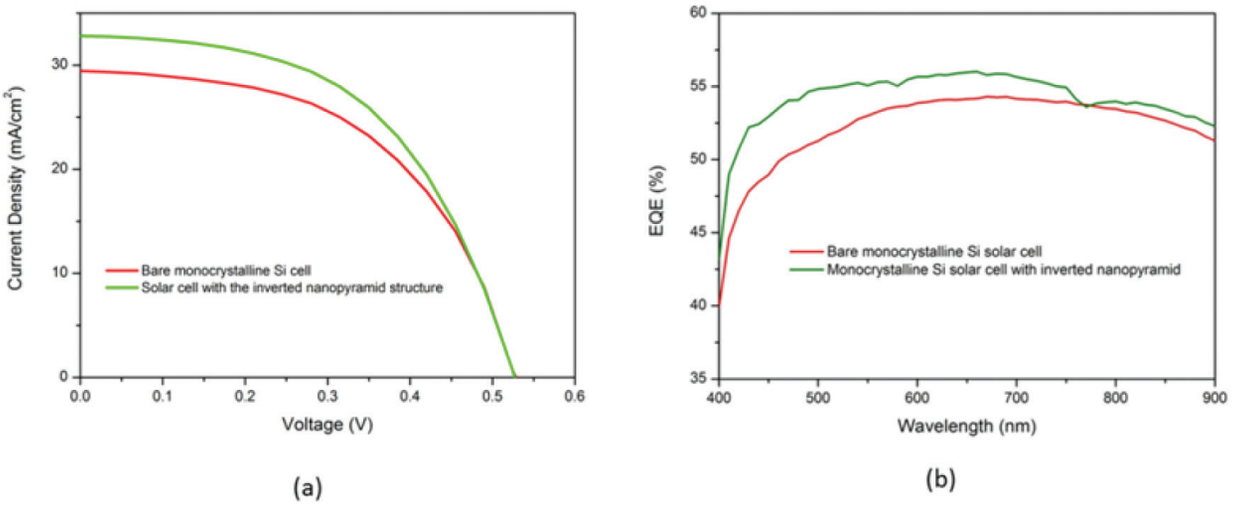

Figure 13. (a) Current density-voltage (J-V) characteristics and (b) EQE spectra of a monocrystalline Si solar cell with and without the inverted nanopyramid structures.

These results demonstrate that the periodic inverted nanopyramid structures reduced the reflections, increased the short-circuit current and improved the efficiency of the monocrystalline silicon solar cells under this study. This is due to the formation of a gradual refractive index gradient between air and the solar cell, which can reduce the Fresnel reflectance and direct more incident light inside the solar cell active layer. The combined light trapping and antireflection effect have been improved, and the optical path length has been prolonged by the inverted nanopyramid structures resulting in increasing the overall conversion efficiency of the monocrystalline Si solar cells. In addition, the nanopyramid coating can be applied after the solar cell fabrication is completed to eliminate any losses due to surface damage by the etching processes for example [45].

Monocrystalline Si solar cells	V_{OC} (V)	J_{SC} (mAcm^{-2})	FF (%)	PCE (%)
Without nanopyramid	0.525	29.442	52.55	8.122
With nanopyramid	0.58	32.793	52.71	9.075

Table 2. Device characteristics of monocrystalline Si solar cells coated with glass with and without the inverted nanopyramid structures.

3.3. Surface wettability

In outdoor environments, solar cells are exposed to the elements and can be easily contaminated by dust particles which interfere with incident light affecting the cell light absorption and thus, reducing the device performance. Therefore, self-cleaning properties at the front surface of the solar cell would maintain the cell performance when exposed to dusty environments [40, 41].

Figure 14 shows the contact angle values of water droplets measured on the planar solar cell, inverted nanopyramid patterned solar cell and SAM-coated inverted nanopyramid patterned solar cell. As shown in **Figure 14**, the contact angle of the solar cell was increased from 55 to

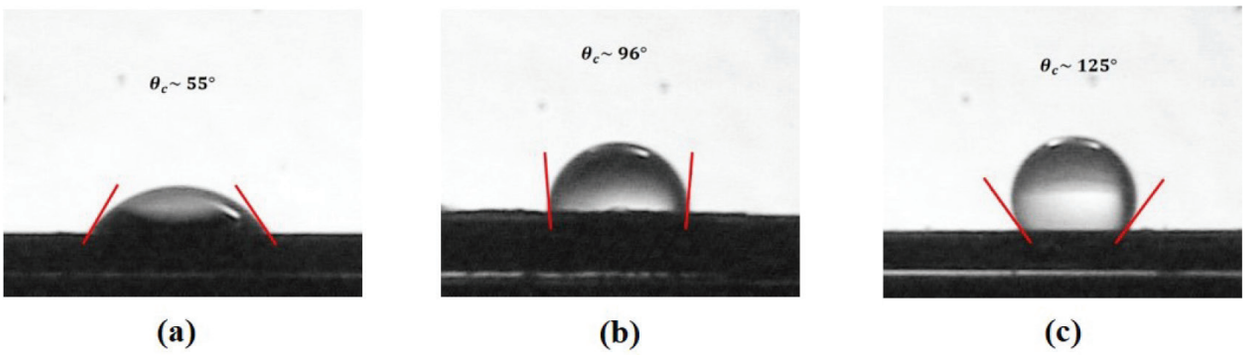

Figure 14. Photographs of a water droplet on: (a) planar solar cell, (b) patterned solar cell with nanopyramids and (c) SAM-coated patterned solar cell. θ c is the water contact angle.

96° after the formation of inverted nanopyramid structure, which exhibited a hydrophobic behavior. Moreover, the hydrophobicity was enhanced with SAM-coated inverted nanopyramid structures. In this case, the contact angle of the SAM-coated patterned solar cell was increased to 125°. As a result, solar cells with inverted nanopyramids can utilize the self-cleaning functionality induced by the high hydrophobic surface properties in addition to the utilization of their antireflection properties.

4. Conclusions

In this chapter, periodic upright and inverted nanopyramid structures were utilized as light-trapping and self-cleaning nanostructures. Low-cost, high-resolution LIL and UV-NIL technologies were used to fabricate the master mold and form these structures. The performance of the solar cells was improved in terms of overall efficiency and reduced reflections. In addition, a superhydrophobic property of the nanopyramids was explored in terms of adding a self-cleaning functionality to the front side encapsulation. The inverted nanopyramid structures were fabricated on Si substrate by LIL and subsequent pattern transfer process using reactive ion etching followed by KOH wet etching. The periodic inverted nanopyramid structures on a silicon substrate were used as a master mold for the imprint process. During the first nanoimprint process, the upright nanopyramid structures were fabricated on the glass substrate by simple, high-throughput and low-cost UV-NIL using Si master mold with inverted nanopyramid structures. The upright nanopyramid structured glass substrates were tested for protective cover glass for solar cell applications and were utilized as a mold for the second imprint process used to form the inverted pyramids.

The diffuse transmittance and haze ratio values were significantly increased for the upright nanopyramid patterned glass, especially, in the wavelength range 300–600 nm compared to the bare glass. This indicates that antireflection and strong light-scattering functions are obtained due to the upright nanopyramid graded refraction index structures. The use of upright nanopyramid structured glass as a cover glass lead to improve the power conversion efficiency of the encapsulated monocrystalline Si solar cell by about 10.97%. This is mainly

due to the increased light scattering and prolongs the optical path length caused by the upright nanopyramid structures compared to the reference cells with bare glass. In addition, the fluorinated upright nanopyramid structured cover glass exhibited larger contact angle (θ_{CA} ~ 132°) and excellent self-cleaning properties.

In the second nanoimprint process, the periodic inverted nanopyramid structures were fabricated on the monocrystalline solar cell front surface using a UV-NIL. The pyramid coating can be applied after cell fabrication to eliminate any losses due to surface damage by the etching processes. The inverted nanopyramid structures decreased the reflectance and increased the external quantum efficiency over a broad wavelength range. The periodic inverted nanopyramid structure has successfully reduced the Fresnel reflection and led to directing and trapping more incident light into the monocrystalline Si solar cells, thereby improving the short-circuit current density and enhancing the power conversion efficiency. The power conversion efficiency of the monocrystalline Si solar cell with inverted nanopyramid structures was improved by 11.73% compared to the planar solar cell. Moreover, the surface of the solar cells exhibited hydrophobic properties due to increased contact angle caused by the nanostructure patterns and the self-assembled monolayer coating. The enhanced hydrophobicity provided the solar cells with an added self-cleaning functionality. These results suggest that the periodic inverted nanopyramid and upright nanopyramid structures with light-harvesting and self-cleaning properties have considerable potential for various types of solar cells and optical systems in real outdoor environments.

Author details

Amalraj Peter Amalathas* and Maan M. Alkaisi

*Address all correspondence to: amalraj.peteramalathas@pg.canterbury.ac.nz

Department of Electrical and Computer Engineering, MacDiarmid Institute for Advanced Materials and Nanotechnology, University of Canterbury, Christchurch, New Zealand

References

[1] Chattopadhyay S, Huang Y, Jen Y-J, Ganguly A, Chen K, Chen L. Anti-reflecting and photonic nanostructures. Materials Science and Engineering: R: Reports. 2010;**69**:1-35. DOI: 10.1016/j.mser.2010.04.001

[2] Söderström K, Escarré J, Cubero O, Haug FJ, Perregaux S, Ballif C. UV-nano-imprint lithography technique for the replication of back reflectors for n-i-p thin film silicon solar cells. Progress in Photovoltaics: Research and Applications. 2011;**19**:202-210. DOI: 10.1002/pip.1003

[3] Wang B, Gao T, Leu PW. Broadband light absorption enhancement in ultrathin film crystalline silicon solar cells with high index of refraction nanosphere arrays. Nano Energy. 2016;**19**:471-475. DOI: 10.1016/j.nanoen.2015.10.039

[4] Hsu CM, Battaglia C, Pahud C, Ruan Z, Haug FJ, Fan S, Ballif C, Cui Y. High-efficiency amorphous silicon solar cell on a periodic nanocone back reflector. Advanced Energy Materials. 2012;**2**:628-633. DOI: 10.1002/aenm.201100514

[5] Moreno M, Daineka D, i Cabarrocas PR. Plasma texturing for silicon solar cells: From pyramids to inverted pyramids-like structures. Solar Energy Materials and Solar Cells. 2010;**94**:733-737. DOI: 10.1016/j.solmat.2009.12.015

[6] Li Y, Zhang J, Yang B. Antireflective surfaces based on biomimetic nanopillared arrays. Nano Today. 2010;**5**:117-127. DOI: 10.1016/j.nantod.2010.03.001

[7] Kanamori Y, Sasaki M, Hane K. Broadband antireflection gratings fabricated upon silicon substrates. Optics Letters. 1999;**24**:1422-1424. DOI: 10.1364/Ol.24.001422

[8] Amalathas AP, Alkaisi MM. Enhancing the performance of solar cells with inverted nanopyramid structures fabricated by UV nanoimprint lithography. In: 2016 IEEE 43rd Photovoltaic Specialists Conference (PVSC). IEEE; 2016. pp. 0346-0349. DOI: 10.1109/PVSC.2016.7749608

[9] Amalathas AP, Alkaisi MM. Periodic upright nanopyramid fabricated by ultraviolet curable nanoimprint lithography for thin film solar cells. International Journal of Nanotechnology. 2017;**14**:3-14. DOI: 10.1504/Ijnt.2017.082435

[10] Wu W, Hu M, Ou FS, Li Z, Williams RS. Cones fabricated by 3D nanoimprint lithography for highly sensitive surface enhanced Raman spectroscopy. Nanotechnology. 2010;**21**:255502. DOI: 10.1088/0957-4484/21/25/255502

[11] Amalathas AP, Alkaisi MM. Efficient light trapping nanopyramid structures for solar cells patterned using UV nanoimprint lithography. Materials Science in Semiconductor Processing. 2017;**57**:54-58. DOI: 10.1016/j.mssp.2016.09.032

[12] Hulteen JC, Van Duyne RP. Nanosphere lithography: A materials general fabrication process for periodic particle array surfaces. Journal of Vacuum Science & Technology A. 1995;**13**:1553-1558. DOI: 10.1116/1.579726

[13] Cheng JY, Ross CA, Thomas EL, Smith HI, Vancso GJ. Fabrication of nanostructures with long-range order using block copolymer lithography. Applied Physics Letters. 2002; **81**:3657-3659. DOI: 10.1063/1.1519356

[14] Guo LJ. Nanoimprint lithography: Methods and material requirements. Advanced Materials. 2007;**19**:495-513. DOI: 10.1002/adma.200600882

[15] Puglisi RA, Garozzo C, Bongiorno C, Di Franco S, Italia M, Mannino G, Scalese S, La Magna A. Molecular doping applied to Si nanowires array based solar cells. Solar Energy Materials and Solar Cells. 2015;**132**:118-122. DOI: 10.1016/j.solmat.2014.08.040

[16] Lu Y, Lal A. High-efficiency ordered silicon nano-conical-frustum array solar cells by self-powered parallel electron lithography. Nano letters. 2010;**10**:4651-4656. DOI: 10.1021/nl102867a

[17] Tsui KH, Lin Q, Chou H, Zhang Q, Fu H, Qi P, Fan Z. Low-cost, flexible, and self-cleaning 3D Nanocone anti-reflection films for high-efficiency photovoltaics. Advanced Materials. 2014;**26**:2805-2811. DOI: 10.1002/adma.201304938

[18] Sivasubramaniam S, Alkaisi MM. Inverted nanopyramid texturing for silicon solar cells using interference lithography. Microelectronic Engineering. 2014;**119**:146-150. DOI: 10.1016/j.mee.2014.04.004

[19] Lin Q, Hua B, Leung S-F, Duan X, Fan Z. Efficient light absorption with integrated nanopillar/nanowell arrays for three-dimensional thin-film photovoltaic applications. ACS Nano. 2013;**7**:2725-2732. DOI: 10.1021/nn400160n

[20] Ferry VE, Sweatlock LA, Pacifici D, Atwater HA. Plasmonic nanostructure design for efficient light coupling into solar cells. Nano Letters. 2008;**8**:4391-4397. DOI: 10.1021/nl8022548

[21] Luo L-B, Xie C, Wang X-H, Yu Y-Q, Wu C-Y, Hu H, Zhou K-Y, Zhang X-W, Jie J-S. Surface plasmon resonance enhanced highly efficient planar silicon solar cell. Nano Energy 2014;**9**:112-120. DOI: 10.1016/j.nanoen.2014.07.003

[22] Jiao F, Huang Q, Ren W, Zhou W, Qi F, Zheng Y, Xie J. Enhanced performance for solar cells with moth-eye structure fabricated by UV nanoimprint lithography. Microelectronic Engineering. 2013;**103**:126-130. DOI: 10.1016/j.mee.2012.10.012

[23] Jorgensen G, Terwilliger K, DelCueto J, Glick S, Kempe M, Pankow J, Pern F, McMahon T. Moisture transport, adhesion, and corrosion protection of PV module packaging materials. Solar Energy Materials and Solar Cells. 2006;**90**:2739-2775. DOI: 10.1016/j.solmat.2006.04.003

[24] Shin JH, Han KS, Lee H. Anti-reflection and hydrophobic characteristics of M-PDMS based moth-eye nano-patterns on protection glass of photovoltaic systems. Progress in Photovoltaics: Research and Applications. 2011;**19**:339-344. DOI: 10.1002/pip.1051

[25] Verma LK, Sakhuja M, Son J, Danner A, Yang H, Zeng H, Bhatia C. Self-cleaning and antireflective packaging glass for solar modules. Renewable Energy. 2011;**36**:2489-2493. DOI: 10.1016/j.renene.2011.02.017

[26] Son J, Kundu S, Verma LK, Sakhuja M, Danner AJ, Bhatia CS, Yang H. A practical superhydrophilic self cleaning and antireflective surface for outdoor photovoltaic applications. Solar Energy Materials and Solar Cells. 2012;**98**:46-51. DOI: 10.1016/j.solmat.2011.10.011

[27] Battaglia C, Escarré J, Söderström K, Charrière M, Despeisse M, Haug F-J, Ballif C. Nanomoulding of transparent zinc oxide electrodes for efficient light trapping in solar cells. Nature Photonics. 2011;**5**:535-538. DOI: 10.1038/Nphoton.2011.198

[28] Ferry VE, Verschuuren MA, MCv L, Schropp RE, Atwater HA, Polman A. Optimized spatial correlations for broadband light trapping nanopatterns in high efficiency ultrathin film a-Si: H solar cells. Nano letters. 2011;**11**:4239-4245. DOI: 10.1021/nl202226r

[29] Gwon HJ, Park Y, Moon CW, Nahm S, Yoon S-J, Kim SY, Jang HW. Superhydrophobic and antireflective nanograss-coated glass for high performance solar cells. Nano Research. 2014;**7**:670-678. DOI: 10.1007/s12274-014-0427-x

[30] Han K-S, Lee H, Kim D, Lee H. Fabrication of anti-reflection structure on protective layer of solar cells by hot-embossing method. Solar Energy Materials and Solar Cells. 2009;**93**:1214-1217. DOI: 10.1016/j.solmat.2009.01.002

[31] Leem JW, Yu JS. Artificial inverted compound eye structured polymer films with light-harvesting and self-cleaning functions for encapsulated III–V solar cell applications. RSC Advances. 2015;**5**:60804-60813. DOI: 10.1039/c5ra05991g

[32] Amalathas AP, Alkaisi MM. Upright nanopyramid structured cover glass with light harvesting and self-cleaning effects for solar cell applications. Journal of Physics D: Applied Physics. 2016;**49**:465601. DOI: 10.1088/0022-3727/49/46/465601

[33] Song YM, Choi HJ, Yu JS, Lee YT. Design of highly transparent glasses with broadband antireflective subwavelength structures. Optics Express. 2010;**18**:13063-13071. DOI: 10.1364/OE.18.013063

[34] Lee SH, Leem JW, Yu JS. Transmittance enhancement of sapphires with antireflective subwavelength grating patterned UV polymer surface structures by soft lithography. Optics Express. 2013;**21**:29298-29303. DOI: 10.1364/OE.21.029298

[35] Dudem B, Leem JW, Lim JH, Lee SH, Yu JS. Multifunctional polymers with biomimetic compound architectures via nanoporous AAO films for efficient solar energy harvesting in dye-sensitized solar cells. RSC Advances. 2015;**5**:90103-90110. DOI: 10.1039/c5ra16276a

[36] Janthong B, Moriya Y, Hongsingthong A, Sichanugrist P, Konagai M. Management of light-trapping effect for a-Si: H/μc-Si: H tandem solar cells using novel substrates, based on MOCVD ZnO and etched white glass. Solar Energy Materials and Solar Cells. 2013;**119**:209-213. DOI: 10.1016/j.solmat.2013.06.045

[37] Ho C-H, Lien D-H, Chang H-C, Lin C-A, Kang C-F, Hsing M-K, Lai K-Y, He J-H. Hierarchical structures consisting of SiO_2 nanorods and p-GaN microdomes for efficiently harvesting solar energy for InGaN quantum well photovoltaic cells. Nanoscale. 2012;**4**:7346-7349. DOI: 10.1039/C2NR32746E

[38] Lin C-A, Lai K-Y, Lien W-C, He J-H. An efficient broadband and omnidirectional light-harvesting scheme employing a hierarchical structure based on a ZnO nanorod/Si_3N_4-coated Si microgroove on 5-inch single crystalline Si solar cells. Nanoscale. 2012;**4**:6520-6526. DOI: 10.1039/C2NR32358C

[39] Qi B, Wang J. Fill factor in organic solar cells. Physical Chemistry Chemical Physics. 2013;**15**:8972-8982. DOI: 10.1039/c3cp51383a

[40] Lee SH, Han KS, Shin JH, Hwang SY, Lee H. Fabrication of highly transparent self-cleaning protection films for photovoltaic systems. Progress in Photovoltaics: Research and Applications. 2013;**21**:1056-1062. DOI: 10.1002/pip.2203

[41] Kim YD, Shin JH, Cho JY, Choi HJ, Lee H. Nanosized patterned protective glass exhibiting high transmittance and self-cleaning effects for photovoltaic systems. Physica Status Solidi (a). 2014;**211**:1822-1827. DOI: 10.1002/pssa.201330643

[42] Cassie A, Baxter S. Wettability of porous surfaces. Transactions of the Faraday Society. 1944;**40**:546-551. DOI: 10.1039/TF9444000546

[43] Tserepi A, Vlachopoulou M, Gogolides E. Nanotexturing of poly (dimethylsiloxane) in plasmas for creating robust super-hydrophobic surfaces. Nanotechnology. 2006;**17**:3977. DOI: 10.1088/0957-4484/17/15/062

[44] Park K-C, Choi HJ, Chang C-H, Cohen RE, McKinley GH, Barbastathis G. Nanotextured silica surfaces with robust superhydrophobicity and omnidirectional broadband super-transmissivity. ACS Nano. 2012;**6**:3789-3799. DOI: 10.1021/nn301112t

[45] Kumaravelu G, Alkaisi M, Bittar A, MacDonald D, Zhao J. Damage studies in dry etched textured silicon surfaces. Current Applied Physics. 2004;**4**:108-110. DOI: 10.1016/j.cap.2003.10.008